Journal of Applied Physics

Long-range structure of Cu (In x Ga 1 − x) 3 Se 5 : A complementary neutron and anomalous x-ray diffraction study

S. Lehmann, D. Fuertes Marrón, M. León, R. Feyerherm, E. Dudzik, E. J. Friedrich, M. Tovar, Y. Tomm, C. Wolf, S. Schorr, Th. Schedel-Niedrig, M. Ch. Lux-Steiner, and J. M. Merino

Articles you may be interested in

Electric-field-induced strain mechanisms in lead-free 94 % (Bi 1 / 2 Na 1 / 2) TiO 3 – 6 % BaTiO 3
Appl. Phys. Lett. **98**, 082901 (2011); 10.1063/1.3557049

Simultaneous changes of nuclear and magnetic structures across the morphotropic phase boundary in (1 − x) BiFeO 3 − xPbTiO 3
Appl. Phys. Lett. **97**, 262506 (2010); 10.1063/1.3533665

Synthesis, magnetic properties, and neutron diffraction study of the complex perovskites R (Cu 3 − x Mn x) Mn 4 O 12 (R = Pr , Nd and x = 1 , 2)
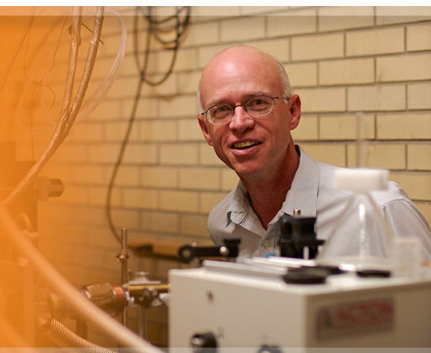J. Appl. Phys. **108**, 083905 (2010); 10.1063/1.3498807

Neutron powder diffraction study and magnetic properties in LaMn 1 − x Cu x O 3 (x = 0.05 , 0.10 and 0.15)
J. Appl. Phys. **107**, 09D719 (2010); 10.1063/1.3358621

Evolution of short-range to long-range monoclinic order of M B type with decreasing temperature in 0.75 [Pb (Mg 1 − 3 Nb 2 − 3) O 3] - 0.25 Pb Ti O 3
J. Appl. Phys. **99**, 076105 (2006); 10.1063/1.2188047

Long-range structure of Cu(In$_x$Ga$_{1-x}$)$_3$Se$_5$: A complementary neutron and anomalous x-ray diffraction study

S. Lehmann,[1,a] D. Fuertes Marrón,[2] M. León,[3] R. Feyerherm,[1] E. Dudzik,[1] E. J. Friedrich,[3] M. Tovar,[1] Y. Tomm,[1] C. Wolf,[1] S. Schorr,[4] Th. Schedel-Niedrig,[1] M. Ch. Lux-Steiner,[1] and J. M. Merino[3]

[1]*Helmholtz-Zentrum Berlin für Materialien und Energie, Hahn-Meitner-Platz 1, 14109 Berlin, Germany*
[2]*Instituto de Energía Solar-ETSIT, Universidad Politécnica de Madrid, 28040 Madrid, Spain*
[3]*Departamento de Física Aplicada, Universidad Autónoma de Madrid, Módulo 12, 28049 Madrid, Spain*
[4]*Institute of Geological Sciences, Free University Berlin, Malteserstr. 74-100, 12249 Berlin, Germany*

Distinguishing the scattering contributions of isoelectronic atomic species by means of conventional x-ray- and/or electron diffraction techniques is a difficult task. Such a problem occurs when determining the crystal structure of compounds containing different types of atoms with equal number of electrons. We propose a new structural model of Cu(In$_x$Ga$_{1-x}$)$_3$Se$_5$ which is valid for the entire compositional range of the CuIn$_3$Se$_5$–CuGa$_3$Se$_5$ solid solution. Our model is based on neutron and anomalous x-ray diffraction experiments. These complementary techniques allow the separation of scattering contributions of the isoelectronic species Cu$^+$ and Ga^{3+}, contributing nearly identically in monoenergetic x-ray diffraction experiments. We have found that CuIII$_3$Se$_5$ (III =In,Ga) in its room temperature near-equilibrium modification exhibits a modified stannite structure (space group $I\bar{4}2m$). Different occupation factors of the species involved, Cu$^+$, In^{3+}, Ga^{3+}, and vacancies have been found at three different cationic positions of the structure (Wyckoff sites 2a, 2b, and 4d) depending on the composition of the compound. Significantly, Cu$^+$ does not occupy the 2b site for the In-free compound, but does for the In-containing case. Structural parameters, including lattice constants, tetragonal distortions, and occupation factors are given for samples covering the entire range of the CuIn$_3$Se$_5$–CuGa$_3$Se$_5$ solid solution. At the light of the result, the denotation of Cu-poor 1:3:5 compounds as chalcopyrite-related materials is only valid in reference to their composition. © *2011 American Institute of Physics*. [doi:10.1063/1.3524183]

I. INTRODUCTION

A controversial and long-term discussion about structural models for Cu-poor, chalcopyrite-related compounds can be followed in the literature.[1–6] The focus lies on the Cu-poor regions of the Cu(In,Ga)Se$_2$–(In,Ga)$_2$Se$_3$ pseudo-binary cuts of the corresponding quaternary Cu–Ga–In–Se phase diagram. Particularly, 1:3:5 and 1:5:8 stoichiometries had a large impact on the discussion and attracted the interest of both experimentalists and theoreticians.[6–9] However, these corporate efforts in understanding and describing the structural properties of the Cu-poor, chalcopyrite-related compounds resulted in a noticeable gap between their concepts. On the one hand theoreticians predicted a defect-complex-related superstructure. According to *ab initio* calculations[6–8] ordered arrays of neutral defect complexes $[2V_{Cu}^- +(Ga,In)_{Cu}^{2+}]^0$ are formed due to favorable energetics and lead to the term of ordered vacancy compounds.[6–8,10] On the other hand, aside from the lack of consensus around a single structural model, facilitated to some extent by the problem of similar scattering powers from isoelectronic species in some of these compounds, no conclusive experimental evidence of the ordered vacancy model could be proved.

The interest in these compounds goes along that of chal-copyrite counterparts, which are well known as efficient pho-tovoltaic materials, providing the highest conversion effi-ciencies of nowadays thin-film photovoltaic devices.[11] The number of relevant publications about Cu-poor, off-1:1:2 stoichiometric compounds drastically increased when a near-surface compositional analysis of a Cu(In,Ga)Se$_2$ solar cell absorber layer revealed indications of such a phase.[12] Al-though the issues related to solar cell devices will not be discussed here in further detail, the results of this investiga-tion might well have certain relevance on particular aspects of high-efficiency chalcopyrite-based thin-film solar cells.

In this contribution we have studied the crystalline struc-ture of the compounds CuIn$_3$Se$_5$, CuGa$_3$Se$_5$, and the corre-sponding quaternaries Cu(In$_x$Ga$_{1-x}$)$_3$Se$_5$, with x from 0 to 1. As a result of this study, we present a new model based on the modified stannite structure for the entire family of 1:3:5 compounds. Following a twofold strategy, we first focused on the synthesis of the material with well defined, near-equilibrium structural properties. This part will not be dis-cussed in detail here, as the relevant information can be found elsewhere.[13,14] Second, the structural parameters of the samples as a function of their composition were extracted from full-pattern analysis of neutron powder diffraction ex-periments, while the occupation factors were obtained from a combination of neutron and anomalous x-ray diffraction (XRD) methods. One aspect is of special importance for a

a)Electronic mail: sebastian.lehmann@ftf.lth.se.

TABLE I. Wyckoff sites and corresponding structure factors of relevant tetragonal superstructure reflections of the stannite-type space group $I\bar{4}2m$.

Wyckoff site	Coordinates	Wyckoff site	Coordinates	hkl	Structure factor
2a	$(0,0,0),(1/2,1/2,1/2)$	8i	$(x,x,z),(x+1/2,x+1/2,z+1/2)$	110	$F_{hkl} \approx 2f_{2a}+2f_{2b}-4f_{4d}$
2b	$(0,0,1/2),(1/2,1/2,0)$		$(-x,-x,z),(-x+1/2,-x+1/2,z+1/2)$	202	$F_{hkl} \approx 2f_{2a}+2f_{2b}-4f_{4d}$
4d	$(0,1/2,1/4),(1/2,0,3/4)$		$(x,-x,-z),(x+1/2,-x+1/2,-z+1/2)$	211	$F_{hkl} \approx 2f_{2a}-2f_{2b}$
	$(0,1/2,3/4),(1/2,0,1/4)$		$(-x,x,-z),(-x+1/2,x+1/2,-z+1/2)$	114	$F_{hkl} \approx 2f_{2a}+2f_{2b}-4f_{4d}$

conclusive structural characterization of these compounds, namely, the distinction of scattering contributions of the iso-electronic species Cu^+ and Ga^{3+}, which is, by itself, a challenging task and almost impossible to solve with standard x-ray and electron diffraction techniques. We have combined neutron and anomalous XRD and we will show that this strategy is fruitful as a means to differentiate scattering contributions of isoelectronic species Cu^+ and Ga^{3+}.

II. EXPERIMENTAL

A. Sample preparation and basic quality testing

$Cu(In_xGa_{1-x})_3Se_5$ powder samples with compositions covering the entire range of the corresponding solid solution (x from 0 to 1) were synthesized from the elements, copper, indium, gallium, and selenium (5N provided by Alfa Aesar). The elemental ingots were weighed, transferred into glassy-carbon boats and introduced in silica glass ampoules which were evacuated before sealing. Anion deficiency was prevented by adding elemental selenium in excess to every ingot. The adjustment of homogeneous compositional and near-equilibrium structural properties was achieved by applying a twofold synthesis regime to the samples. First, the ingots were heated up to 1000 °C and partially above the melting point, kept there for 4 h and subsequently cooled down to room temperature, with a cooling rate of approximately 300–400 °C/h down to 400 °C. Second, a homogenization step followed, including mortaring of the material, which was afterwards pressed into tablets and again placed in sealed, evacuated silica glass ampoules with a pellet of selenium. Annealing for four to six weeks at 650 °C completed the synthesis. For detailed information about sample preparation and the impact of the annealing and annealing temperature on the compositional and structural properties of the samples see Ref. 13.

Prior to the diffraction study, preliminary quality checks of the synthesized powders were carried out. For compositional analysis, we used inductively coupled-plasma mass-spectrometry (ICP-MS), in a Sciex Elan 6000 system provided by Perkin-Elmer, and total x-ray fluorescence (T-XRF) in a Cameca 8030C system, followed by qualitative phase analysis by XRD measurements in a Bruker D8 Advance system, using Cu $K_{\alpha1/2}$ radiation and the DIFFRAC PLUS software package for data analysis. Standard reference materials silicon (SRM 640b) and lanthanum hexaboride (SRM 660a),[15] measured under identical conditions as the powders, served for an accurate XRD system calibration.

B. Neutron and anomalous x-ray powder diffraction

The neutron powder diffraction experiments were carried out at the E9 high resolution neutron powder diffractometer at BERII (Ref. 16) using a wavelength of $\lambda = 1.797$ Å. For the room temperature measurements, the powders were placed in vanadium containers, together with an Y_2O_3 (Ref. 15) powder standard. The latter served as a reference for setup calibration.

Anomalous XRD experiments at ambient temperature were carried out at the MAGS beamline[17] at the Berlin synchrotron radiation source BESSY. The samples were mixed with Corundum (Al_2O_3) reference powder[15] and placed into evacuated fused silica capillaries with a diameter of 500 μm. Coarse-grain effects were avoided by sample rotation. For the anomalous diffraction experiments five different x-ray energies were chosen close to and off the Cu (8979 eV) and Ga (10367 eV) K-edges. The diffracted x-rays were recorded using a two-dimensional charge-coupled device (CCD) detector. Data for constant scattering angles were integrated numerically using the software package FIT2D provided by ESRF.[18]

The evaluation of both neutron and anomalous XRD measurements was carried out with the FULLPROF software package by Rodriguez-Carvajal[19] and followed the Rietveld method.[20] The atomic x-ray scattering factors, necessary for the simulation of anomalous XRD data, were estimated according to the CROMER–LIBERMAN (Ref. 21) code, provided by Ref. 22.

A few preliminary considerations were necessary in order to figure out suitable Bragg peaks for the anomalous diffraction experiment. In general, the intensity of a Bragg reflection is proportional to the square of the structure factor, which is the sum of the scattering contributions of each lattice site of the crystallographic unit cell times its characteristic, element-specific scattering power f_i for the applied probe. The general formalism is given below [Eq. (1)]. In the space group $I\bar{4}2m$, the stannite type structure of the copper-poor compounds is characterized by four independent crystallographic sites which are defined by their fractional coordinates (Table I). The structure factors can be derived from these positions [Eq. (2)]. The denotation of Eq. (2) leaves the assignment of the cationic sites f_{2a}, f_{2b}, and f_{4d} to the species Cu^+, In^{3+}, Ga^{3+}, and vacancies free, while we assume that the 8i site is fully occupied by selenium.

$$F_{hkl} = \sum_i f_i[e^{2\pi i(hx+ky+lz)}], \qquad (1)$$

TABLE II. X-ray scattering factor contributions f_{i0}, f_i', f_i'' for Cu^+, Ga^{3+}, In^{3+}, and Se, as used in the simulations for the XRD measurements, following the CROMER–LIBERMAN code,[21,22] for Q-values of the corresponding 202 and 211 reflections of $CuGa_3Se_5$ and $Cu(In_{0.33}Ga_{0.66})_3Se_5$ (a) and for energy values close to and off the copper and gallium K-edges (b).

	(a)					(b)							
	Cu^+	Ga^{3+}	In^{3+}	Se		Cu^+		Ga^{3+}		In^{3+}		Se	
Q (Å^{-1})	f_0	f_0	f_0	f_0	E (eV)	f′	f″	f′	f″	f′	f″	f′	f″
	$CuGa_3Se_5$					Copper K-edge							
2.551_{202}	23.49	24.70	39.51	26.78	8 600	−2.84	0.52	−1.59	0.69	−0.10	4.51	−1.01	1.01
2.611_{211}	23.32	24.56	39.26	26.59	8 979	−10.41	0.48	−1.79	0.64	−0.10	4.19	−1.11	0.94
	$Cu(In_{0.33}Ga_{0.66})_3Se_5$					Gallium K-edge							
2.513_{202}	23.60	24.79	39.67	26.91	10 000	−1.33	3.24	−2.99	0.52	−0.16	3.49	−1.40	0.77
2.572_{211}	23.43	24.65	39.42	26.71	10 367	−0.99	3.06	−11.65	0.49	−0.19	3.28	−1.52	0.72

$$F_{hkl} = f_{2a}[1 + e^{\pi i(h+k+l)}] + f_{2b}[e^{\pi i(l)} + e^{\pi i(h+k)}]$$
$$+ f_{4d}[(e^{\pi i(k+l/2)}) + (e^{\pi i(h+3l/2)}) + (e^{\pi i(k+3l/2)})$$
$$+ (e^{\pi i(h+l/2)})] + f_{Se}[(e^{2\pi i(hx+kx+lz)})$$
$$+ (e^{\pi i\{h(2x+1)+k(2x+1)+l(2z+1)\}}) + (e^{2\pi i(-hx-kx+lz)})$$
$$+ (e^{\pi i\{h(1-2x)+k(1-2x)+l(2z+1)\}})] + f_{Se}[(e^{2\pi i(hx-kx-lz)})$$
$$+ (e^{\pi i\{h(2x+1)+k(1-2x)+l(1-2z)\}}) + (e^{2\pi i(-hx+kx-lz)})$$
$$+ (e^{\pi i\{h(1-2x)+k(2x+1)+l(1-2z)\}})]. \quad (2)$$

Using Eq. (2), we have identified a pair of Bragg reflections, namely, 202 and 211, which appeared most suitable for the anomalous XRD experiments (Table I—two discarded reflections are also shown additionally). Their Bragg angles are close but their structure factors $F_{202} \approx 2f_{2a} + 2f_{2b} - 4f_{4d}$ and $F_{211} \approx 2f_{2a} - 2f_{2b}$, respectively, depend quite differently on the occupations of the different Wyckoff sites (the contribution of selenium to the structure factor is neglected as it almost cancels out when the anion site parameters x_{Se} and z_{Se} found by neutron diffraction are used). In addition, they are also close to the Al_2O_3 104 Bragg reflection which served as an internal energy and intensity reference. The x-ray scattering factor f_i is both element-specific and energy dependent—two characteristic properties we will use to determine the occupation factors of the $Cu(In_xGa_{1-x})_3Se_5$ compounds, and can be written as follows:

$$f_i = f_{i0} + f_i' + if_i''.$$

Estimated values of the three contributions to f_i were calculated using the CROMER–LIBERMAN code[21,22] and are given in Table II for the individual species involved and for energies both at and slightly off the Cu–K and Ga–K absorption edges. While there are no large differences between the f_0 values for Cu^+ and Ga^{3+}, the respective value for In^{3+} shows a reasonably strong contrast with respect to these ions. The contrast between Cu^+ and Ga^{3+}, however, is strongly increased close to the respective K-edge absorption edges at 8979 eV and 10367 eV, respectively. Here, significant differences in f_i' and f_i'' can be observed and any energy dependent changes of Bragg intensities will be exclusively due to the respective species. Notably, significant changes of the rela-

tive intensities of the 202/211 pair of Bragg reflections are expected when varying the energy.

C. Previous structural models and material synthesis

A variety of different structural models was proposed for both, $CuIn_3Se_5$ and $CuGa_3Se_5$,[1–6,13] as summarized in Table III. Similarities among the proposals include (i) the assignment to the tetragonal crystallographic system, (ii) the assumption of an anionic sublattice fully populated by Se^{2-}, and (iii) the assumption that the species Cu^+, In^{3+}, Ga^{3+}, and related vacancies occupy the cationic sublattice. Differences between the proposed models refer to (i) the choice of different space groups, resulting in different extinction rules for diffraction experiments, (ii) random or ordered occupation of (iii) two to six symmetrically independent cation-related Wyckoff sites, and finally (iv) varying anion displacements from the ideal position, x_{Se}, y_{Se}, and z_{Se}. The latter issue critically depends on the choice of the space group and the occupation of neighboring cation-related lattice sites. Nevertheless, not only the structural differences are obvious from Table III but so are the variety of analysis techniques and synthesis regimes followed in reported works. Stemming from the characteristic sensitivity of the different investigation methods and preparation recipes utilized, major difficulties in the interpretation of structural characterization follow. As an example, experiments concluding in anomalous occupation factors of the cationic lattice sites (see Table III), might be related to incomplete temperature treatments of the samples. The resulting occupations differ from room-temperature equilibrium distributions and lead to minor differences in low intensity Bragg reflections, barely or not even detectable by means of standard diffraction techniques. Hence, it is generally not straightforward to decide at the light of simple diffraction experiments whether or not the compounds investigated have reached near-equilibrium structural properties. We conclude that probably most of the enumerated material properties of a given compound can be attributed to the issue of the synthesis regime, a conclusion we have recently reported about for pure $CuGa_3Se_5$ and $CuIn_3Se_5 - CuGa_3Se_5$ alloy samples.[13,14]

TABLE III. (Color online) Structural parameters, models, and synthesis methods of Cu-poor, chalcopyrite-related compounds with 1:3:5 and 1:5:8 stoichiometries, as reported in literature.
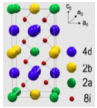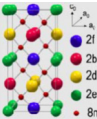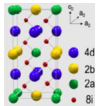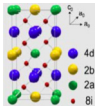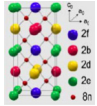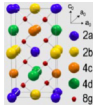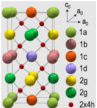
Denotation	Space group	Structural data — multiplicity and Wyckoff sites, coordinates (x,y,z), and occupation per unit cell					Unit cell	Synthesis	Analysis technique	Reference

Structural models for $CuGa_3Se_5$ and related compounds

Denotation	Space group	Wyckoff	x	y	z	occupation	Unit cell	Synthesis	Analysis technique	Reference
Stannite ($CuGa_3Se_5$)	$I\bar{4}2m$ (121)	2a	0	0	0	$0.47(2)Cu^+$,		From 5N elements Annealed for 1008 h at 650 °C	Combined neutron and synchrotron powder diffraction study including Rietveld refinement	13
		2b	0	0	1/2	$2.00(5)Ga^{3+}$				
		4d	0	1/2	1/4	$1.15(9)Cu^+, 2.79(8)Ga^{3+}$				
		8i	x	x	z	$7.9(2)Se^{2-}$				
P-chalcopyrite ($CuGa_3Se_5$, $CuGa_5Se_8$)	$P\bar{4}2c$ (112)	2b	1/2	0	1/4	Not given		From 5N elements Annealed for 48 h at 660 °C		1
		2d	0	1/2	1/4					
		2e	0	0	0					
		2f	1/2	1/2	0					
		8n	x	y	z					

Structural models for $CuIn_3Se_5$ and related compounds

Denotation	Space group	Wyckoff	x	y	z	occupation	Unit cell	Synthesis	Analysis technique	Reference
Stannite-I ($CuIn_3Se_5$)	$I\bar{4}2m$ (121)	2a	0	0	0	$1.6Cu^+$		Synthesized from the binaries (Cu_2Se, In_2Se_3) Annealed at 700 °C for 24–168 h	Selected area electron diffraction in transmission electron microscopy (TEM)	2
		2b	0	0	1/2	$0.8In^{3+}$				
		4d	0	1/2	1/4	$4.0In^{3+}$				
		8i	x	x	z	$8.0Se^{2-}$				
Stannite-II ($CuIn_3Se_5$)	$I\bar{4}2m$ (121)	2a	0	0	0	$0.54Cu^+$		Synthesized from 6N elements by vertical Bridgman method Cooled from 750 °C to 500 °C (5 K/h)	Standard powder XRD and Rietveld refinement	3
		2b	0	0	1/2	$1.73In^{3+}$				
		4d	0	1/2	1/4	$1.02Cu^+, 2.98In^{3+}$				
		8i	x	x	z	$8.00Se^{2-}$				
P-chalcopyrite ($CuIn_3Se_5$)	$P\bar{4}2c$ (112)	2b	1/2	0	1/4	$1.80(8)Cu^+$		From the elements Annealed for 480 h at 750 °C Quenched in H_2O	Single crystal x-ray diffraction	4
		2d	0	1/2	1/4	$2.00In^{3+}$				
		2e	0	0	0	$1.36(6)Cu^+$				
		2f	1/2	1/2	0	$1.12(4)In^{3+}$				
		8n	x	y	z	$7.20(32)Se^{2-}$				
Thiogallate ($CuIn_3Se_{5.3}$)	$I\bar{4}$ (82)	2a	0	0	0	$0.8Cu^+$		Material prepared from 5N elements Ingots used for CVT $T_{Growth}=760$ °C (168 h) and cooled to RT	Selected area electron diffraction in TEM	5
		2b	0	0	1/2	$2.0In^{3+}$				
		2c	0	1/2	1/4	$2.0In^{3+}$				
		2d	0	1/2	3/4	$0.2Cu^+$				
		8g	x	y	z	$8.0Se^{2-}$				
Ordered vacancy-/ defect compound ($CuIn_{3-5}Se_{5-8}$)	$P\bar{4}$ (81)	1a	0	0	0	$1.0Cu^+$		Derived from *ab initio* calculations		6
		1b	0	0	1/2	$1.0III^{3+}$				
		1c	1/2	1/2	0	$1.0III^{3+}$				
		1d	1/2	1/2	1/2	$0.8III^{3+}$				
		2g	0	1/2	z	$0.6Cu^+$				
		2g	0	1/2	z	$2.0III^{3+}$				
		4h	x	y	z	$8.0Se^{2-}$				

TABLE IV. Compositional data obtained from ICP-MS of samples of the solid solution series $Cu(In,Ga)_3Se_5$. The nominal composition, equivalent to the sample denotation, is given in the left column while the measured composition appears in the right column. The error of the ICP-MS was estimated to be 1 at. % absolute (only given for the sum formulae). Lattice parameters a_0 and c_0, as well as the tetragonal distortion $\eta = c_0/2a_0$ yielded by Rietveld analysis of neutron diffraction are also included.

Sample (initial weight)	Measured	a_0 (Å)	c_0 (Å)	η
$CuIn_3Se_5$	$Cu_{1.0(1)}In_{3.1(1)}Se_{5.0}$	5.756(1)	11.530(2)	1.0017(3)
$Cu(In_{0.9}Ga_{0.1})_3Se_3$	not analyzed	5.740(1)	11.508(2)	1.0024(3)
$Cu(In_{0.8}Ga_{0.2})_3Se_5$	$Cu_{1.1(1)}In_{2.5(1)}Ga_{0.6(1)}Se_{5.0}$	5.715(1)	11.435(1)	1.0005(3)
$Cu(In_{0.66}Ga_{0.33})_3Se_5$	$Cu_{0.9(1)}In_{2.0(1)}Ga_{1.1(1)}Se_{5.0}$	5.673(1)	11.335(2)	0.9991(3)
$Cu(In_{0.6}Ga_{0.4})_3Se_5$	not analyzed	5.663(1)	11.304(2)	0.9980(3)
$Cu(In_{0.5}Ga_{0.5})_3Se_5$	$Cu_{0.9(1)}In_{1.5(1)}Ga_{1.5(1)}Se_{5.0}$	5.637(1)	11.241(2)	0.9969(3)
$Cu(In_{0.33}Ga_{0.66})_3Se_5$	$Cu_{1.0(1)}In_{1.0(1)}Ga_{2.1(1)}Se_{5.0}$	5.598(1)	11.127(2)	0.9938(3)
$Cu(In_{0.2}Ga_{0.8})_3Se_5$	$Cu_{1.1(1)}In_{0.6(2)}Ga_{2.5(1)}Se_{5.0}$	5.571(1)	11.054(2)	0.9921(3)
$CuGa_3Se_5$	$Cu_{0.9(1)}Ga_{3.0(1)}Se_{5.0}$	5.518(1)	10.950(2)	0.9921(3)

III. RESULTS AND DISCUSSION

Following the preparation procedure described briefly in the experimental section above and extensively studied in Refs. 13 and 14, high quality material was prepared for the present study. According to ICP-MS compositional analysis, the stoichiometry of the investigated samples was in good agreement with the weighed elemental ingot material, as shown in Table IV. All powders were single-phase, as revealed by x-ray powder diffraction analysis and no miscibility gap among the two phases $CuIn_3Se_5$ and $CuGa_3Se_5$ could be observed, in agreement with previous reports.[23] The high crystalline quality of the sample material was derived from full width at half maximum (FWHM) values of the XRD patterns, which were of the same order of those of Si and LaB_6 reference material[15] (FWHM $\approx 0.2°$ in 2θ at a diffraction angle of $2\theta \approx 70°$).

A. Rietveld refinement of neutron diffraction data: Structural parameters

As commented in the introduction section, neutron diffraction offers the intrinsic advantage of separating scattering contributions of isoelectronic species Cu^+ and Ga^{3+}. In a first approach, the space group and structural parameters, such as lattice constants a_0, c_0, tetragonal distortion η, anion site parameters x_{Se}, y_{Se}, and z_{Se}, and the unit cell volume were extracted by full pattern Rietveld refinements from the neutron powder diffraction data. According to this analysis, the entire $Cu(In_xGa_{1-x})_3Se_5$ solid solution exhibits a stannite-type structure $I\bar{4}2m$ (space group no. 121), which implies four symmetrically independent lattice sites 2a, 2b, 4d, and 8i. The assignment to this space group followed after running the Rietveld refinement with all structural models published so far and summarized in Table III as input parameters. After several iterations and special refinement procedures,[24] the resulting parameter sets were compared among each other, considering quality criteria (e.g., R_{Bragg}, $R_{weighted\ profile}$, and χ^2), structural parameters, and isotropic Debye–Waller factors (B_{iso}). The best agreement, implying lowest figures of quality factors and meaningful structural parameters (e.g., avoiding over-occupation of lattice sites or unphysical—

either too large or negative—values of the isotropic Debye–Waller factors), was achieved when using the stannite-type structure as an input. The good congruence between the experiment and the deduced structural model is reflected by the low intensity residual spectra in Fig. 1. Here the neutron diffraction data, final Rietveld refinements, and residuals are given for five selected $Cu(In_xGa_{1-x})_3Se_5$ samples.

Independently of the results obtained from Rietveld refinements of neutron diffraction data, a space group search was carried out by means of the routines DICVOL04 (Ref. 25) and CHECKGROUP included in the FULLPROF suite.[19] The highest figures of merit were achieved for a set of proposed solutions which are all listed in Table III and hence tested.

An important issue regarding the deduced space group $I\bar{4}2m$, is the fact that no direct relation exists with the chalcopyrite space group $I\bar{4}2d$, according to symmetrical super- and/or subgroup relations.[26] Only indirect relations exist between these space groups via the thiogallate $I\bar{4}$ or via the $I\bar{4}$, $P\bar{4}$, and $P\bar{4}2c$ symmetries. It is, therefore, implied that the denotation of the Cu-poor 1:3:5 compounds as chalcopyrite-
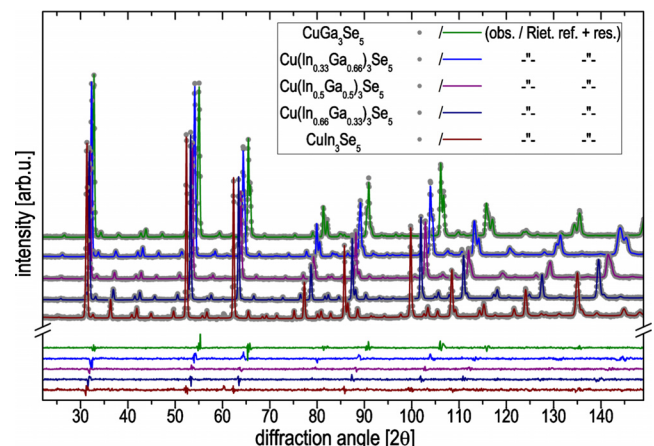

FIG. 1. (Color online) Experimental neutron powder diffractograms (gray circles), Rietveld refinements (solid lines top), and the corresponding residuals (solid lines bottom) of $Cu(In_xGa_{1-x})_3Se_5$ samples covering the entire solid solution range, with an increasing gallium content from bottom to top.
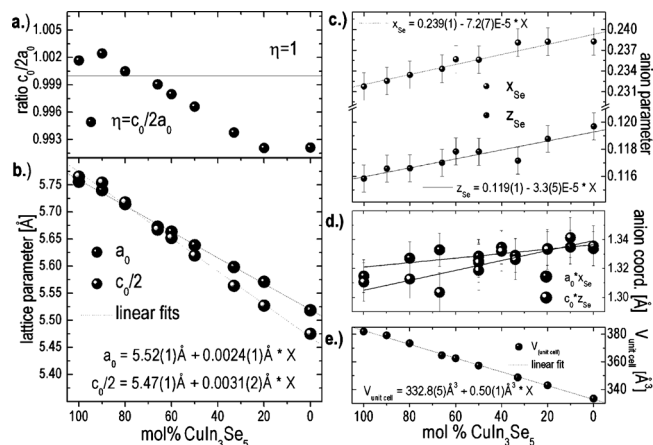
FIG. 2. Tetragonal distortion $\eta = c_0/2a_0$ (a), lattice constants a_0 (black) and $c_0/2$ (gray) (b), anion site parameters x_{Se} and z_{Se} (c), anion coordinates (d), and unit cell volume (e) of the $Cu(In_xGa_{1-x})_3Se_5$ solid solution series, as determined by Rietveld analysis of neutron powder diffraction data assuming stannite-type structure. Linear fits are included in (b)–(e). For tetragonal distortion values in (a), the solid line, represents, as a guide to the eye, the pseudocubic case $\eta = 1$.

related materials is solely correct when referring to compositional issues but not in terms of the symmetry of the crystal structure.

Concerning the structural parameters, Fig. 1 shows an increase in the lattice parameters a_0 and c_0 for increasing amounts of $CuIn_3Se_5$, as prominent Bragg reflections shift toward lower diffraction angles. This is due to the preservation of the crystal structure and the difference in ionic radii of the interalloy substituted species, $In^{3+}(0.62$ Å$)$ and $Ga^{3+}(0.47$ Å$)$. The ionic radii are given for tetrahedral coordination and charges (Ref. 27) as present in the compounds studied here.

Values of a_0 and c_0 were extracted from the Rietveld refinements (included in Fig. 1) and are shown in Table IV together with the tetragonal distortion parameter $\eta = c_0/2a_0$ The distortional parameter η describes the compression or elongation of the unit cell along the c-axis ([001]-direction) with respect to the quasi-cubic case. This results in Bragg reflection splitting of prominent doublets for nonpseudocubic cases $(\eta \neq 1)$, as observed, e.g., for 220/204, 312/116, 400/008 doublets (see Fig. 1) and becomes more pronounced at higher diffraction angles. The peak splitting decreases for In richer compounds as the distortion is generally reduced and even vanishes for a distinct [In]/[Ga]-ratio $(x \approx 0.75)$. Figure 2 summarizes the extracted structural parameters and shows their composition dependent behavior: η [Fig. 2(a)], a_0 and $c_0/2$ [Fig. 2(b)], the anion site parameters x_{Se} and z_{Se} [Fig. 2(c)], the anion coordinates [Fig. 2(d)], and finally the unit cell volume [Fig. 2(e)]. The assigned lattice parameters a_0 and c_0 are in good agreement with previously reported data[1–6,13,28,29] but nevertheless, minor deviations in tetragonal distortion values are noticeable, likely related to different methods of material synthesis used, as mentioned above. Both a_0 and $c_0/2$ [Fig. 2(b)] show a linear increase with In-enrichment [Fig. 2(b)], following Vegard's law, as can also be noticed in the unit cell volume [Fig. 2(e)]. However, uneven slopes characterize the composition-dependence of a_0

and $c_0/2$, which leads to a crossing point of both graphs. This is the case for contents of approximately 25 ± 3 mol % $CuGa_3Se_5$ alloyed in $CuIn_3Se_5$, the pseudocubic case for a vanishing tetragonal deformation. Generally, the values of η are close to one, reflecting only minor deviations from the nondistorted case, with a compressed unit cell for $CuGa_3Se_5$ and an expanded cell for $CuIn_3Se_5$.

Another set of characteristic structural quantities are the anion site parameters x_{Se} and z_{Se}. In the present case, defined by the fundamental symmetry operations of the established space group $I\bar{4}2m$, the two positions x_{Se} and y_{Se} are symmetrically equivalent, and only x_{Se} is needed for a complete description of the crystal structure. These values define the position of selenium anions as ratios of the fundamental lattice parameters a_0 (x_{Se}) and c_0 (z_{Se}) along the corresponding directions of the crystal lattice. For a nondistorted, pseudocubic unit cell, x_{Se} and z_{Se} would adopt values of $(1/4)a_0$ and $(1/8)c_0 = (2\eta a_0/8)$, respectively, comparable to the case of the cubic $F\bar{4}3m$ supergroup counterpart of the sphalerite-type structure. Plotted versus composition [Fig. 2(c)], a linear dependency of x_{Se} and z_{Se} following Vegard's law can be noted. Also the absolute coordinates of the anionic lattice sites in angstrom [Fig. 2(d)] follow a linear decrease for indium enrichment with different slopes for $a_0 \times x_{Se}$ and $c_0 \times z_{Se}$, respectively.

Notably, the position of selenium is shifted approximately along $[\bar{2}\bar{2}\bar{1}]$ toward 2a $(0,0,0)$ when alloying more and more $CuIn_3Se_5$ into $CuGa_3Se_5$. This was concluded from the linear decrease in $a_0 \times x_{Se}$ and $c_0 \times z_{Se}$ for increasing amounts of indium in Fig. 2(d). Although we have not discussed the occupation factors of the corresponding Wyckoff sites in the crystal structure yet, we can anticipate at this point that the 2a position is only occupied by approximately one quarter of Cu^+ and three quarters of vacancies, whereas the other two positions are shared, at least fractionally, by Ga^{3+} and In^{3+}. According to the differences in ionic radii[27] and reported bond distances, as well as ionicities of the pairs $In^{3+}-Se^{2-}$ and $Ga^{3+}-Se^{2-}$ in the chalcopyrite counterparts (Ref. 30 and references within), the resulting shift in the selenium position toward the 2a site can be explained in a twofold way. First intrinsically reduced Cu^+-Se^{2-} bond distances, as in In-rich chalcopyrite compounds (Ref. 30 and references within) and second the depletion of Cu^+ (and the corresponding vacancy enrichment) on the 2a site. Both issues may favor the spatial relaxation of the polyhedron with the observed consequences. However, neutron diffraction probes long-range ordering only, and the observed values reflect the distances between lattice sites, not the bond distance situations as probed by short-range sensitive methods like, e.g., extended x-ray absorption fine structure (EXAFS) (Refs. 30 and references within, and[31,32]). Nevertheless, the distances between lattice sites obtained from neutron diffraction adopt composition-dependent values which are in good agreement with corresponding $In^{3+}-Se^{2-}$ and $Ga^{3+}-Se^{2-}$ bond lengths as reported for the chalcopyrite counterparts with locally resolved techniques (Ref. 30 and references within).
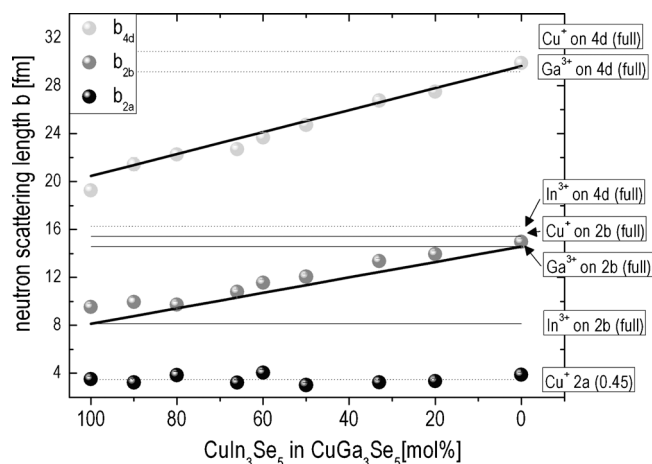
FIG. 3. Neutron scattering lengths of the 2a (black), 2b (gray), and 4d (light gray) positions of the stannite-type structure extracted from Rietveld refinements of the neutron powder diffractograms. Assignments are given, corresponding to full occupation of the 2b (solid) and 4d (dotted/top) sites with either Cu^+, Ga^{3+}, or In^{3+} and for the 2a (dotted/bottom) site filled with $Cu^+(0.45)$. For the 2b and 4d sites additional extrapolations are given, following an occupation according to the compositional $[Ga^{3+}]/[In^{3+}]$-ratio, without Cu^+ on 2b and with $1.15Cu^+$ on 4d.

B. Rietveld refinement of neutron diffraction data: Occupation factors

The next step after having determined the complete set of fundamental structural parameters for the entire $Cu(In_xGa_{1-x})_3Se_5$ solid solution is to quantify the contributions of the involved species Cu^+, In^{3+}, Ga^{3+}, Se^{2-}, and related vacancies on the predefined lattice sites. Three different Wyckoff sites are occupied by four different cationic species—including vacancies, as deduced from the stannite-type structural model proposed for these compounds. The 1:3:5 stoichiometry, therefore, translates into a unit cell content of 1.6:4.8:8, and thus $1.6Cu^+$ and 4.8 (In^{3+}, Ga^{3+}) distribute over the available eight cation sites. This also shows that 1.6 vacancies per unit cell are present. The isoelectronic character of Cu^+ and Ga^{3+} is hindering, if not even making it impossible, to separate the scattering contributions of these two species by techniques in which the probe interacts with the electonic shell of the species, like standard x-ray or electron diffraction. The nuclear interaction responsible of neutron diffraction permits the distinction of isoelectronic species with different mass numbers, as the neutron scattering lengths are in principle different. With values for the involved elements of $b_{Cu} = 7.718(4)$ fm, $b_{Ga} = 7.228(2)$ fm, $b_{In} = 4.065(20)$ fm, and $b_{Se} = 7.970(9)$ fm,[33] the distinction between Cu^+ and Ga^{3+} is possible though still a challenging task. In a first approach we solely calculated the integral (=multiplicity × average) neutron scattering length of the 2a, 2b, and 4d Wyckoff sites (Fig. 3), instead of having three times more variables in the calculation when allowing all three cations to occupy all available lattice sites. The results are given in Fig. 3 and allowed a qualitative estimation of probable occupations of the cationic lattice sites. Horizontal lines in Fig. 3 indicate the calculated scattering lengths for full and partial occupation of lattice sites.

A unique behavior was found for the 2a position which shows a composition-independent result of average 3.5 fm.

With respect to the tabulated values for Cu^+, Ga^{3+}, and In^{3+}, this is far below a full occupation with any of these species, which suggests that the vacancies are dominantly located on the 2a site. The independence from composition suggests that neither Ga^{3+} nor In^{3+} is involved in the occupation of the 2a site. We conclude with respect to the integral value of the neutron scattering length, that $0.45Cu^+$ per unit cell are located on the 2a site, thus the 2a site is filled by approximately one quarter copper and three quarters vacancies.

A different situation holds for the 2b site. First of all, the scattering lengths are, in contrast to the 2a site, composition-dependent and adopt higher values for decreasing amounts of $CuIn_3Se_5$, pointing to increased occupation factors. Copper can be excluded as an exclusive candidate on this site as this would imply an occupation of 60% to 95%, according to the calculated scattering lengths. This exceeds the entire amount of copper present in the compounds, even for the lowest of estimated percentage values. The direct correlation between the increase in the scattering length and the depletion of indium is a strong hint for a mixed Ga^{3+} and In^{3+} population, apart from other possible involved species. As a guide to the eye a line is shown in Fig. 3 which corresponds to the full occupation of the 2b site with Ga^{3+} and In^{3+} at ratios corresponding to the overall composition of the respective compounds. However, the experimental data adopt, in either case, higher values than the extrapolated ones. This can be explained in two ways, (i) Cu^+ is partly involved in the occupation of the 2b site, while In^{3+} and Ga^{3+} are providing the residual material with a ratio corresponding to the composition of the respective compound or (ii) the $[In]/[Ga]$ ratio is always lower than the overall value for the corresponding compound, if only these two species are present. These cases are hard to distinguish. Nevertheless, the likelihood of the first assumption (i) was confirmed from the complete Rietveld refinements discussed below.

For the 4d site the trend of the composition dependence is similar to that for the 2b site, indicating a direct correlation between the $[In]/[Ga]$ ratio of the compound and the $[In]/[Ga]$ ratio of the occupancy factors. Likewise plotted for 2b, a line in Fig. 3 corresponds to the neutron scattering length for an $[In]/[Ga]$ ratio similar to the respective compound, assuming that $1.15Cu^+$ per unit cell reside on the 4d site as an exclusive In^{3+} and Ga^{3+} occupation can be excluded. A fairly good agreement can be observed when comparing this interpolation with the experimentally determined values. A possible interpretation of the observed results is: Cu^+, In^{3+}, and Ga^{3+} occupy the 4d site with a constant amount of copper and a compound-dependent $[In]/[Ga]$-ratio exactly reflecting the overall ratios of the respective compounds. Nevertheless, an unambiguous conclusion about the occupation scenarios could not be drawn.

However, the question arises if the scattering length present at the cationic sublattice is generally overestimated, as revealed by the deviations observed for the 2b site. On the one hand this could be linked to selenium depletion—because a full anion sublattice occupation was assumed. A collective downward shift in the integral scattering lengths in Fig. 3 would be the result. On the other hand, an excess of
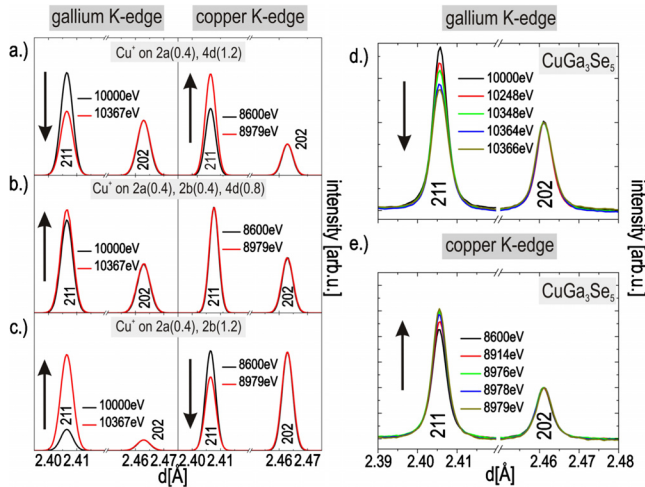
FIG. 4. (Color online) Simulations [(a)–(c)] and measurements [(d) and (e)] of $CuGa_3Se_5$ 202 and 211 Bragg reflections, the latter normalized to the 202 intensity. Experimental data correspond to anomalous XRD off- and close to the copper and gallium K-edges, at different excitation energies, 8600–8979 eV and 10 000–10 367 eV, respectively. Simulations assume $CuGa_3Se_5$ exhibiting stannite-type structure with three different Cu^+ arrangements at Wyckoff sites 2a, 2b, and 4d: copper occupies (a) the 2a (0.4) and 4d (1.2) sites, (b) the 2a (0.4), 2b (0.4), and 4d (0.8) sites, and (c) the 2a (0.4) and 2b (1.2) sites.

copper could also lead to the observed results but was likewise not confirmed by the compositional analysis.

In summary, from neutron diffraction data alone it was not possible to unambiguously determine quantitatively the occupation factors of the individual species for the three distinct cationic sites present in the stannite-type structural crystal lattice of the $Cu(In_xGa_{1-x})_3Se_5$ compounds, except for the Ga-free ternary $CuIn_3Se_5$. We attributed this to the comparatively small difference in the neutron scattering lengths of Cu^+ and Ga^{3+} and the sensitivity and/or resolution limits of the neutron diffraction experiment. As a concluding result, the question was simplified to: "To what fraction does Cu^+ finally occupy the 2b site?"

C. Occupation factors obtained from combining anomalous x-ray and neutron diffraction

Anomalous XRD was selected as a complementary method to determine unambiguously the occupancy factors at cationic sites, and therefore, which of the copper distribution scenario discussed above represents the actual solution of the problem. Using this technique, the x-ray scattering factors of individual atoms can be tuned separately, as they are energy-dependent and element-specific.

For the discussion of the results we begin with the In-free ternary $CuGa_3Se_5$. Figure 4 shows the experimental data sets of the 202/211 Bragg reflections, recorded in the energy ranges of the Ga K- [Fig. 4(d)] and Cu K-absorption edges [Fig. 4(e)]. The right panels of Fig. 4 show details of the corresponding simulations for four different energies—close to (black) and directly at (red) the Ga K-edge (left) and Cu K-edge (right) [Figs. 4(a)–4(c), respectively]. In order to answer the question stated at the end of the previous section— "To what fraction does Cu^+ finally occupy the 2b site?"—, three different Cu^+ distributions on the Wyckoff sites 2a, 2b,

and 4d were considered for these simulations: (i) Cu^+ only on 2a and 4d, (ii) Cu^+ on 2a, 2b, and 4d, i.e., a gradual redistribution of Cu from 4d to 2b, and (iii) Cu^+ only on 2a and 2b. Despite the fact that case (iii) was already excluded, it is still considered in order to estimated the tendency of the Cu^+ occupation on the 2b site—no Cu [case (i)], a partial Cu^+ occupation [case (ii)], and a full Cu^+ occupation [case (iii)]. For clarity, each individual data set, experimental as well as calculated, are shown normalized to the 202 peak. The simulated diffractograms in Figs. 4(a)–4(c) show the two characteristic features used for the qualitative evaluation, namely, the general trend of the intensity ratio $[I_{211}]/[I_{202}]$ when approaching the Ga and Cu K-edges (emphasized by arrows in the graphs) and the numerical values of $[I_{211}]/[I_{202}]$.

For case (i) [Fig. 4(a)] where Cu^+ occupies the 2a and 4d site with occupation factors of 0.4 (2a) and 1.2 (4d) a decrease in the intensity of the 211 peak is simulated at energies close to the Ga K-edge. Correspondingly, an increase in the intensity of the 211 peak occurs at energies close to the Cu K-edge. The $[I_{211}]/[I_{202}]$ intensity ratio, which is in the range of 1.2:1 at the Ga K-edge, appears significantly larger at the Cu K-edge (3.2:1). Figure 4(b) represents the calculations for model (ii) with Cu^+ populating all three cationic sites by equal amounts, 0.4 (2a), 0.4 (2b), and 0.8 (4d). For this case, the energy-dependence of the intensity of the 211 peak is expected at the Ga K-edge but not in the Cu K-edge energy regime. Additionally, the $[I_{211}]/[I_{202}]$ intensity ratio is significantly higher at the Ga K-edge and lower at the Cu K-edge, when compared to the corresponding curves of Fig. 4(a) [case (i)]. The simulation for cases (i) and (ii) show some similarity but the situation drastically changes if Cu^+ is occupying the 2a (0.4) and 2b (1.2) sites only [case (iii)], with the corresponding simulations given in Fig. 2(c). Here a strong intensity increase at the Ga K-edge and a minor decrease at the Cu K-edge are coupled with radically different $[I_{211}]/[I_{202}]$-ratios compared to the previous ones.

In the following we compare the calculated behavior of the intensity of the 211 peak and the $[I_{211}]/[I_{202}]$ intensity-ratio for the three cases with the experimental data obtained at different probe energies. The development of the 211 reflection, measured at a series of excitation energies from 10 000 to 10 367 eV, the latter corresponding to the Ga K-edge, is shown in Fig. 4(d). A clearly detectable decrease in maximum intensity of the 211 reflection, as well as an $[I_{211}]/[I_{202}]$ intensity ratio of approximately 1.9–1.4:1, is observed as the excitation energy approaches that of the Ga K-edge. Compared to the simulations, this behavior agrees well with model (i). This conclusion is additionally strengthened with the corresponding observations at the Cu K-edge, where the excitation energy was swept from 8600 to 8979 eV (the latter corresponding to the Cu K-edge). They also revealed an exclusive matching with model (i), as a slight increase in the 211 maximum intensity and the increase in the $[I_{211}]/[I_{202}]$ intensity ratio associated indicate. The good qualitative agreement between the experimental data and the simulation using the parameters of model (i) led us to reject the other two models (ii) and (iii).
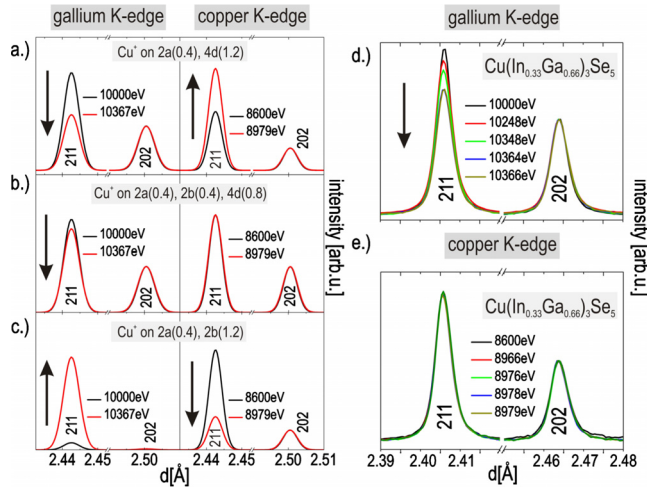
FIG. 5. (Color online) Simulations [(a)–(c)] and measurements [(d) and (e)] of $CuInGa_2Se_5$ 202 and 211 Bragg reflections, the latter normalized to the 202 intensity. Experimental data correspond to anomalous XRD off- and close to the copper and gallium K-edges, at different excitation energies, 8600–8979 eV and 10 000–10 367 eV, respectively. Simulations assume $Cu(In_{0.33}Ga_{0.66})_3Se_5$ exhibiting stannite-type structure with three different Cu^+ arrangements at Wyckoff sites 2a, 2b, and 4d: copper occupies the (a) 2a (0.4) and 4d (1.2) sites, (b) the 2a (0.4), 2b (0.4), and 4d (0.8) sites, and (c) the 2a (0.4) and 2b (1.2) sites.

Similar measurements were carried out on five samples covering the entire compositional range of the quaternary compounds. Since qualitative results are similar and the sensitivity is reduced for a decreasing integral gallium amount, results are presented only for the quaternary compound $Cu(In_{0.33}Ga_{0.66})_3Se_5$ in Fig. 5, as an example for the entire series. The simulations, which are shown in Figs. 5(a)–5(c), were calculated for identical occupational models as those presented for the ternary compound $CuGa_3Se_5$ in Fig. 4, with one exception: In^{3+} and Ga^{3+} are now sharing the trivalent positions with ratios corresponding to the integral composition of the alloy. Compared to the In-free ternary material, a quite similar behavior can be observed in the simulations of model (i), with almost identical maximum intensities of 211 reflections and $[I_{211}]/[I_{202}]$ intensity ratios [Fig. 5(a)]. A reduced sensitivity is obvious from the simulations when accounting for model (ii) [Fig. 5(b)], which is caused by a

decreased integral gallium amount. For this model, the intensity difference at the Ga K-edge is slightly decreased, whereas the tendency in the gallium window and the $[I_{211}]/[I_{202}]$ intensity ratios in both energy ranges are still comparable to the plots of $CuGa_3Se_5$. The simulations for model (iii) [Fig. 5(c)] again show a distinct behavior with an extreme situation—the 202 Bragg reflection almost vanishes. Nevertheless, the general trend is still comparable to the graphs obtained for $CuGa_3Se_5$.

For the quaternary sample $Cu(In_{0.33}Ga_{0.66})_3Se_5$, the collected data are given in Figs. 5(d) and 5(e), measured under identical experimental conditions as the ternary sample of Fig. 4. The best matching with the theoretical model was, contrarily to the case of $CuGa_3Se_5$, observed for model ii. A slight decrease in the 211 peak maximum intensity when approaching the Ga K-edge, no observable changes in the vicinity of the Cu K-edge, as well as almost identical $[I_{211}]/[I_{202}]$ intensity ratios for both energy windows [1.8:1 (Cu-K edge)—2.1:1 (Ga-K edge)], are a clear indication for this finding. According to this result, models i and iii could be excluded for the quaternary compounds. Concerning the quantitative evaluation, unfortunately no precise values can be given. But according to the comparison between the presented simulations and the observed data, the Cu^+ occupational factor at the 2b site can be estimated to adapt a value of 0.4 ± 0.2.

However, establishing one structural model was a highly appreciable result, as it allowed the final, complete Rietveld refinements of the neutron diffraction measurements, including the assignment of occupancy factors for all involved species, Cu^+, In^{3+}, Ga^{3+}, and vacancies. The vacancy distribution is not explicitly indicated, it can be found from the difference of occupation factors and multiplicity. The conclusive results are given in Table V, which includes also the quality factors of the appropriate Rietveld refinements. Both the Rietveld refinements and the corresponding residua reflect the excellent matching of the established structural model and are shown in Fig. 1 for selected compounds. Finally, we found the 2b and 4d sites to be fully occupied while the $[In^{3+}]/[Ga^{3+}]$ ratios at these sites adapt values according to the integral composition of the compounds. The 2a site is

TABLE V. Occupational factors of the 2a, 2b, 4d, and 8i sites of the newly determined modified stannite-type structure of the $Cu(In_xGa_{1-x})_3Se_5$ solid solution series for Cu^+, Ga^{3+} or In^{3+}, and Se^{2-} according to the cationic and anionic sublattices. The occupation factors are given normalized to the multiplicity of the corresponding Wyckoff sites. Selenium was set to full occupation.

Sample $(CuIn_3Se_5)_x$–$(CuGa_3Se_5)_{1-x}$	Occupation of the cationic/anionic sublattice sites									Quality factors		
	2a		2b			4d			8i	R_B	R_{WP}	
	Cu^+	V_{Cu^+}	Cu^+	In^{3+}	Ga^{3+}	Cu^+	In^{3+}	Ga^{3+}	Se^{2-}	(%)	(%)	χ^2
x=1.0	0.47(3)	1.53(3)	0.31(3)	1.83(1)	⋯	0.77(1)	3.16(1)	⋯	8.0	3.6	12.4	1.5
x=0.9	0.46(4)	1.54(4)	0.38(7)	1.43(8)	0.18(7)	0.78(9)	2.88(9)	0.31(9)	8.0	5.2	16.8	2.0
x=0.8	0.48(5)	1.52(5)	0.40(9)	1.30(9)	0.29(9)	0.83(9)	2.63(9)	0.61(9)	8.0	3.7	14.7	1.8
x=0.66	0.42(3)	1.58(3)	0.41(9)	1.24(9)	0.37(9)	0.77(9)	1.95(9)	1.23(9)	8.0	2.9	12.0	1.3
x=0.6	0.54(3)	1.46(3)	0.38(9)	1.14(9)	0.48(9)	0.71(9)	1.82(9)	1.32(9)	8.0	5.2	13.7	1.5
x=0.5	0.41(2)	1.59(2)	0.38(9)	0.94(9)	0.77(9)	0.88(9)	1.52(9)	1.70(9)	8.0	3.8	12.6	1.2
x=0.33	0.41(2)	1.59(2)	0.35(9)	0.49(9)	1.18(9)	0.85(9)	1.10(9)	2.11(9)	8.0	4.8	11.5	1.5
x=0.2	0.47(3)	1.53(3)	0.31(9)	0.14(9)	1.58(9)	0.94(9)	0.86(9)	2.42(9)	8.0	4.9	14.4	1.9
x=0.0	0.47(3)	1.53(3)	⋯	⋯	2.00(5)	1.13(9)	⋯	2.79(8)	8.0	3.4	11.7	1.8

composition independently occupied with 0.45Cu^+ and 1.55 vacancies. For the amount of Cu^+ at 2b and 4d we have to distinguish the In-free and In-containing compounds. For the In-free compound $CuGa_3Se_5$ no copper was found at the 2b site while the residual copper, which was not placed at the 2a site, was determined to occupy the 4d position. In the case of the In-containing compounds a composition-independent amount of 0.35Cu^+ and 0.8Cu^+ were occupying the 2b and 4d sites, respectively.

D. Is there a long-range ordering of vacancies or defect complexes?

Long-range ordering of copper vacancies and related neutral defect complexes $\{2V_{Cu}^- + (Ga, In)_{Cu}^{2+}\}^0$ as proposed after *ab initio* calculations in previous literature reports[6–9,31] was tested. According to these calculations 4 defect complexes are distributed over five unit cells of the 1:3:5 compounds, or in other words 0.8 defect complexes ($\{1.6V_{Cu}^- + 0.8(In, Ga)_{Cu}^{2+}\}^0$) per unit cell $Cu_{1.6}III_{4.8}Se_8$. Such a structure, belonging to space group $P\bar{4}$ should result in occupation fractions of 0.4Cu^+ and 1.6V_{Cu}^- at the 2g Wyckoff site (0,1/2,1/4) and of 0.8 at the 1d site (1/2,1/2,1/2) for the corresponding $(In, Ga)_{Cu}^{2+}$-antisite defects. All investigated samples were thoroughly tested within the refinement procedures in search of any hint pointing to the existence of a superstructure. Results were negative and no evidence of long-range ordering could be found. Small differences in total energies between different orderings of defect complexes (ordered versus nonordered)[8] might well be the key for understanding the experimental findings. Even if short-range ordering of defect pairs was still conserved, a small fraction of disorder could result in the breakup of the superstructure.

IV. CONCLUSIONS

In summary, we have determined that the complete series of $Cu(In_xGa_{1-x})_3Se_5$ compounds (with x=0 to 1) crystallizes in the stannite-type structure, with space group $I\bar{4}2m$, as concluded from neutron and anomalous XRD experiments. The structure model was derived from Rietveld refinements. For this purpose, all previously reported structural models for the family of ternary compounds of comparable compositions were tested. At the light of the result, the denotation of Cu-poor 1:3:5 compounds as chalcopyrite-related materials is only valid in reference to their composition. The space groups of stannite ($I\bar{4}2m$) and chalcopyrite ($I\bar{4}2d$) are not directly related by symmetry to each other, merely indirectly via the thiogallate structure $I\bar{4}$, according to group theoretical considerations. Complete sets of structural parameters, such as lattice constants a_0 and c_0, the unit cell volume, the tetragonal distortion η, the anion site parameters x_{Se} and z_{Se}, and the occupation factors of the Wyckoff sites 2a, 2b, and 4d for the corresponding cationic species were determined. a_0 and c_0, the unit cell volume, the tetragonal distortion, and the anion site parameters show a linear increase with increasing values of the corresponding parameter for increasing indium content—except for the anion coordinates which show a decrease. However, an exception was observed

for the tetragonal distortion of both ternaries as the values do not agree with the linear behavior shown by the quaternary alloys. Both the structural parameters and the occupational factors of $Cu(In_xGa_{1-x})_3Se_5$ compounds are critically dependent on the synthesis parameters. For this reason, we focused on room temperature, near-equilibrium modifications of the compounds, which were thoroughly prepared. According to the combined study of neutron and anomalous x-ray diffraction, the occupational factors of the structure model could finally be determined, as follows:

$CuGa_3Se_5$
Cu^+ and vacancies at 2a,
Ga^{3+} at 2b, and
Cu^+ plus Ga^{3+} at 4d,

$Cu(In_xGa_{1-x})_3Se_5$
Cu^+ and vacancies at 2a,
Cu^+, Ga^{3+}, and In^{3+} at 2b,
and Cu^+, Ga^{3+}, and In^{3+} at 4d,

$CuIn_3Se_5$
Cu^+ and vacancies at 2a,
Cu^+ and In^{3+} at 2b,
and Cu^+ plus In^{3+} at 4d.

Additionally, long-range ordering of neither copper vacancies nor related neutral defect complexes $\{2V_{Cu}^- + (Ga, In)_{Cu}^{2+}\}^0$ could be proved.

[1]G. Marín, S. Tauleigne, S. M. Wasim, R. Guevara, J. M. Delgado, C. Rincón, A. E. Mora, and G. S. Pérez, Mater. Res. Bull. **33**, 1057 (1998).
[2]T. Hanada, A. Yamana, Y. Nakamura, O. Nittono, and T. Wada, Jpn. J. Appl. Phys., Part 2 **36**, L1494 (1997).
[3]W. Paszkowicz, R. Lewandowska, and R. Bacewicz, J. Alloys Compd. **362**, 241 (2004).
[4]W. Hönle, G. Kühn, and U.-C. Boehnke, Cryst. Res. Technol. **23**, 1347 (1988).
[5]B. H. Tseng and C. A. Wert, J. Appl. Phys. **65**, 2254 (1989).
[6]S. B. Zhang, S.-H. Wei, and A. Zunger, Phys. Rev. Lett. **78**, 4059 (1997).
[7]S. B. Zhang, S.-H. Wei, A. Zunger, and H. Katayama-Yoshida, Phys. Rev. B **57**, 9642 (1998).
[8]S. B. Zhang, S.-H. Wei, and A. Zunger, Appl. Phys. Lett. **72**, 3199 (1998).
[9]S.-H. Wei and A. Zunger, J. Appl. Phys. **78**, 3846 (1995).
[10]J. E. Bernard and A. Zunger, Phys. Rev. B **37**, 6835 (1988).
[11]I. Repins, M. A. Contreras, B. Egaas, C. DeHart, J. Scharf, C. L. Perkins, B. To, and R. Noufi, Prog. Photovoltaics **16**, 235 (2008); M. A. Green, K. Emery, Y. Hishikawa, and W. Warta, *ibid.* **17**, 320 (2009).
[12]D. Schmid, M. Ruckh, F. Grunwald, and H. W. Schock, J. Appl. Phys. **73**, 2902 (1993); D. Schmid, M. Ruckh, and H. W. Schock, Appl. Surf. Sci. **103**, 409 (1996).
[13]S. Lehmann, D. Fuertes Marrón, M. Tovar, Y. Tomm, C. Wolf, S. Schorr, T. Schedel-Niedrig, E. Arushanov, and M. Ch. Lux-Steiner, Phys. Status Solidi A **206**, 1009 (2009); S. Lehmann, Ph.D. thesis, Freie Universität Berlin, 2007.
[14]S. Lehmann, D. Fuertes Marrón, J. M. Merino, M. León, E. J. Friedrich, M. Tovar, Y. Tomm, C. Wolf, S. Schorr, T. Schedel-Niedrig, and M. Ch.

Lux-Steiner, *Thin-Film Semiconductor Compounds*, MRS Symposia Proceedings No. 1165 (Materials Research Society, Pittsburgh, 2009), p. M-03–09.

[15] http://ts.nist.gov/MeasurementServices/ReferenceMaterials/

[16] D. M. Többens, N. Stüßer, K. Knorr, H. M. Mayer, and H. Lampert, Proceedings of the Seventh European Powder Diffraction Conference, 2001, Vol. 378–381, pp. 288-293.

[17] E. Dudzik, R. Feyerherm, W. Diete, R. Signorato, and Ch. Zilkens, J. Synchrotron Radiat. **13**, 421 (2006).

[18] http://www.esrf.eu/computing/scientific/FIT2D/

[19] http://www.ill.fr/pages/Science/Diff/Soft/Fp/

[20] H. M. Rietveld, J. Appl. Crystallogr. **2**, 65 (1969).

[21] D. T. Cromer and D. Liberman, Acta Crystallogr., Sect. A: Found. Crystallogr. **37**, 267 (1981); D. T. Cromer and J. T. Waber, Acta Crystallogr. **18**, 104 (1965); D. T. Cromer and J. B. Mann, J. Chem. Phys. **47**, 1892 (1967).

[22] http://usaxs.xor.aps.anl.gov/staff/ilavsky/AtomicFormFactors.html

[23] H. P. Wang, J. Cryst. Growth **200**, 137 (1999).

[24] R. A. Young, *The Rietveld Method* (Oxford University Press, New York, 1995).

[25] A. Boultif and D. Louer, J. Appl. Crystallogr. **37**, 724 (2004).

[26] *International Tables for Crystallography*, Vol. A, Space-group Symmetry, edited by Th. Hahn (Kluwer Academic, Dordrecht, 1999).

[27] R. D. Shannon, Acta Crystallogr., Sect. A: Cryst. Phys., Diffr., Theor. Gen. Crystallogr. **32**, 751 (1976).

[28] J. M. Merino, S. Mahanty, M. León, R. Diaz, F. Rueda, and J. L. Martín de Vidales, Thin Solid Films **361–362**, 70 (2000); J. M. Merino, M. Di Michiel, and M. León, J. Phys. Chem. Solids **64**, 1649 (2003).

[29] J. M. Merino and S. Lehmann (unpublished).

[30] J. M. Merino, R. Díaz, and M. León, Phys. Rev. B **61**, 10211 (2000).

[31] C.-H. Chang, S.-H. Wei, J. W. Johnson, S. B. Zhang, N. Leyarovska, G. Bunker, and T. J. Anderson, Phys. Rev. B **68**, 054108 (2003).

[32] J. M. Merino, S. Díaz-Moreno, G. Subías, and M. León, Thin Solid Films **480–481**, 295 (2005).

[33] A.-J. Dianoux and G. Lander, *Neutron Data Booklet* (ILL, QCP Science imprint, old city publishing group, Philadelphia, 2001).